Influence of double InGaAs/InAs channel on DC and RF performances of InP-based HEMTs

H. L. Hao, M. Y. Su, H. T. Wu, H. Y. Mei, R. X. Yao, F. Liu, H. Wen, S. X. Sun*

School of Information Engineering, Huanghuai University, Zhumadian 463000, China

The double InGaAs/InAs channel structure is designed to improve DC and RF characteristics of InP-based HEMT, which is studied by the numerical simulation. The saturated channel current, transconductance, subthreshold slope, drain induced barrier lowering, and frequency characteristics are analyzed. A comparison is done between the device with the double InGaAs/InAs channel and InGaAs channel. By using double InGaAs/InAs channel, maximum transconductance of 1019.7 mS/mm is achieved, and the lower value of subthreshold slope and drain induced barrier lowering is also obtained. The excellent performance of device with double InGaAs/InAs channel structure is mainly due to the enhanced confinement of the electrons in the channel region. In addition, the maximum oscillation frequency of 758.7 GHz is obtained with the double InGaAs/InAs channel structure.These results indicate that InP-based HEMT with double InGaAs/InAs channel structure is a promising candidate for high frequency application.

(Received February 27, 2022; Accepted May 30, 2022)

Keywords: InP-based HEMT, Double InGaAs/InAs channel structure, DC characteristics, Frequency characteristics

1. Introduction

With the rapid development of high-speed integrated circuits (ICs) and Nano/Micro electro-mechanical system device, the III-V compound semiconductor devices receive more attention due to their superior electrical properties, such as high mobility, high critical breakdown electric field and et.al[1-4]. Among III-V material systems, the much lower noise figures and higher gain performance have been realized for InP-based HEMTs due to the high sheet carrier density, high peak drift velocity, and high electron mobility for the InAlAs/InGaAs material system [5-8]. Therefore, it is widely used in opto-electronic communication systems, millimeter-wave wireless communication systems[9-11].

In recent years, most of researchers are pursuing higher device performance of InAlAs/InGaAs HEMT with different methods. To prevent the DC anomalous effect of InAlAs/InGaAs HEMT, the Si_3N_4/Al_2O_3 stack layer passivation technology was adopted by the

* Corresponding author: sunshuxianga@126.com

https://doi.org/10.15251/JOR.2022.183.411

Ding et al.[12]. After Si_3N_4/Al_2O_3 passivation, the maximum drain current and transconductance reached 800 mA/mm and 1100 mS/mm, respectively. In order to improve the frequency performance, a shorter gate length of InAlAs/InGaAs HEMT was achieved by Ajayan et al., which indicated that the fmax was up to 1460 GHz with 20 nm gate length[13]. To further improve the characteristics of InAlAs/InGaAs HEMT, indium-rich InGaAs channel was a effective method due to the larger conduction band offset and better carrier confinement[14]. Therefore, the double composite channel InP-based HEMT with InGaAs/InAs/InGaAs/InAs/InGaAs is investigated in this paper.

In this work, we propose a InAlAs/InGaAs HEMT with double InGaAs/InAs channel layer to achieve much higher drain current, transconductance and frequency performance. The Sentaurus-TCAD is used to simulate the device structures and characteristics. By adopting the double InGaAs/InAs channel, the maximum drain current of 635.9 mA/mm and maximum transconductance of 1019.7 mS/mm are achieved. Moreover, the f_T and f_{max} are also up to 392.6 GHz and 758.7 GHz for HEMT with double InGaAs/InAs channel, respectively.

2. Device Structure and Model

The schematic of single InGaAs channl (SC) and double InGaAs/InAs channel (DC) HEMTs are shown in Fig. 1. Except for the channel, the structures of SC and DC HEMT are the same.The epitaxial layers each include a 500 nm $In_{0.52}Al_{0.48}As$ buffer layer, a 3 nm $In_{0.52}Al_{0.48}As$ spacer layer and a 15 nm $In_{0.52}Al_{0.48}As$ barrier layer. In addition, the length of the gate and the distance between the source and the drain for both device were set as 100 nm and 2.4 μm, respectively. For SC HEMT, a 15 nm $In_{0.53}Ga_{0.47}As$ is adopted. For DC HEMT, double 3/4/3/4/3 $In_{0.53}Ga_{0.47}As$/InAs/$In_{0.53}Ga_{0.47}As$/InAs/$In_{0.53}Ga_{0.47}As$ channel is adopted to form the multiple quantum wells, leading to confining the electrons at the hetero-interface, and improve the characteristics of device.

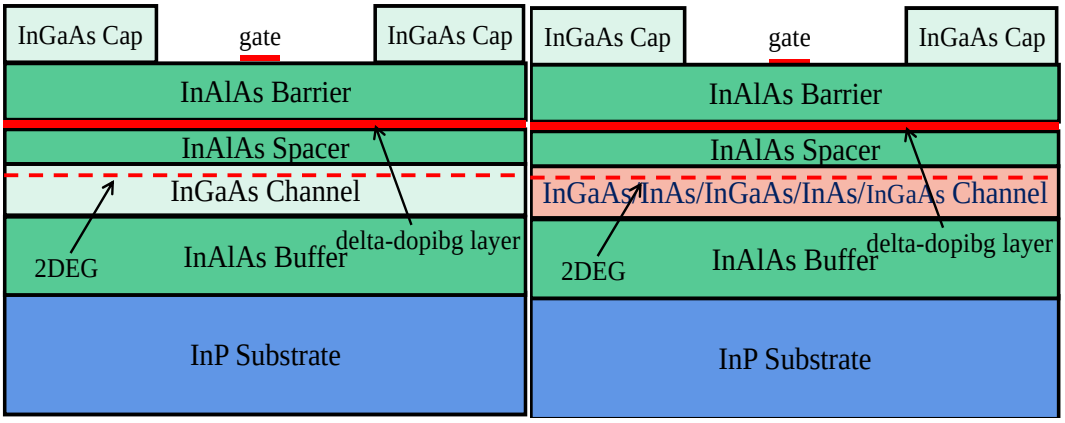

(a) *(b)*

Fig. 1 Schematic structures of (a) SC HEMT and (b) CC HEMT.

In order to make the simulation results more accurate, the reasonable physical model is chosen in the simulation. To describe the carrier transport properties in the channel, the Hydrodynamic transport model is adopted[15]. Due to the quantization effect of 2DEG, the eQuantumPotential model is used[16]. The Arora doping-dependent mobility model and Caneli high field saturation mobility model are used to describe the variation of carrier mobility[17]. For describing the recombination phenomenon, Schockley-Read-Hall, Auger and Radiative recombination model are chosen[18]. Besides, several crucial physical models were also taken into account in the simulation.

The model parameters of InAlAs and InGaAs materials in the simulation are obtained from the Ref [19]. The Newton calculate method is used in the simulation and the temperature is set as 300 K. In addition, the mirror-injection from semi-device structure and the gradient mesh are used to increase the solve speed and convergence problem, respectively[16,19].

3. Results and discussion

The energy band diagrams of three different channel structures under V_{GS}=0 V are shown in Fig. 2 (a). Figure 2 (b) shows the conduction band in the channel region. The vertical cut is done at center of gate electrode. As illustrated Fig. 2, the energy band could be modulated by different channel structure. It was found that the CC channel and DC channel can effectively increase the conduction band. Compared with the SC structure, the depth of potential wells for CC and DC structure were increased by 0.37 eV and 0.39 eV, respectively. This means that the CC and DC structure enhance confinement of the electrons in the channel region. Furthermore, the double electron potential wells were formed for the DC channel. The second potential well would reduce the number of electrons spreading into the InAlAs buffer layer. Therefore, the DC channel structure is more effective in confinement of the electrons than SC and CC channel structure.

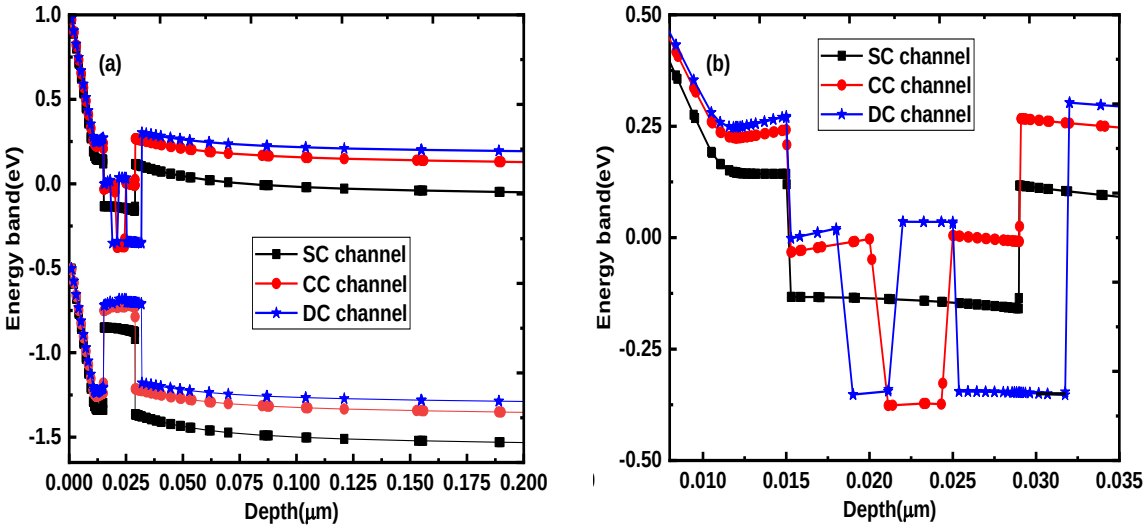

Fig. 2. The energy band diagrams of the single $In_{0.53}GaAs_{0.47}As$ channel(SC HEMT), $In_{0.53}Ga_{0.47}As/InAs/In_{0.53}Ga_{0.47}As$ channel(CC HEMT) and $In_{0.53}Ga_{0.47}As/InAs/In_{0.53}Ga_{0.47}As$ channel(DC HEMT) under V_{GS}=0 V.

Figure 3 shows the electron distributions of the three different structures at V_{GS}=0 V. As observed in Fig. 3, more electrons are distributed in the channel for DC structure. The peak electron concentration of DC HEMT was much higher than the SC HEMT, which resulted in better device characteristics. In addition, a second quantum well was formed due to the second InGaAs/InAs structure. The electrons in the buffer region were much lower than that of SC HEMT and CC HEMT,as shown inset of Fig. 3. Therefore, the DC structure effectively restrained the electrons spilling over the channel.

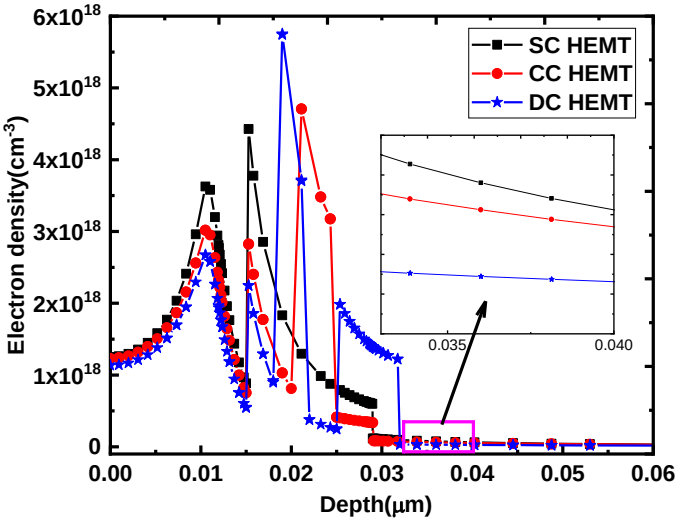

Fig. 3. Electron concentration distributions of SC HEMT, CC HEMT and DC HEM under V_{GS}=0 V.

Figure 4 specifically indicates the map of the electron distribution inside the SC HEMT and DC HEMT. It can be seen that most of electrons were distributed near the InAsAs/InGaAs interface for SC HEMT. For DC HEMT, the peak electrons exited at first InGaAs/InAs interface. This was mainly due to the position of deepest potential well was changed by the different channel structure. It is also clearly observed that the more electrons exited in the buffer region. This result indicated a significant improvement of 2-DEG confinement, which was beneficial from the employment of DC channel structure.

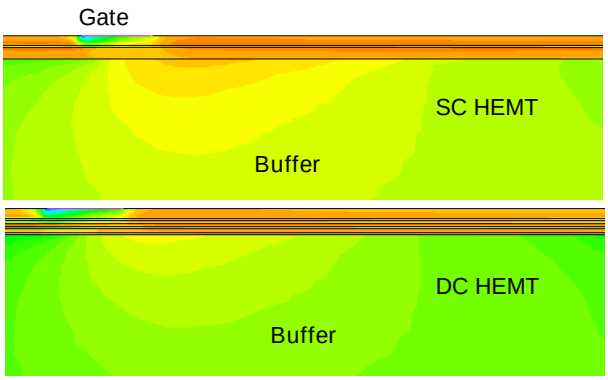

Fig. 4. Electron concentration distributions inside the SC HEMT and DC HEMT.

Figure 5 shows the drain current-voltage curves (I_{DS}-V_{DS}) for CC HEMT and CC HEMT under the gate voltage (V_{GS}) ranged from 0 to -0.4 V with step -0.1 V. As is seen from the figure, the channel current (I_{DS}) of the CC HMET is much larger than that of SC HEMT when the V_{GS} is the same. At V_{GS}=0 V, the saturated channel currents of CC HEMT and SC HEMT are 635.9 mA/mm and 366.8 mA/mm, respectively. Compared with the SC HEMT, the saturated channel current is about 73.4% higher than that of the double InGaAs/InAs CC HEMT. The on-resistance is calculated at V_{GS}=0 V and V_{DS} ranged from 0 to 0.18 V. The on-resistance of CC HEMT is 0.50 Ω•mm and 22% smaller than the SC HEMT. The higher saturated channel current and lower on-resistance are attributed to the superior electron density in the double InGaAs/InAs channel.

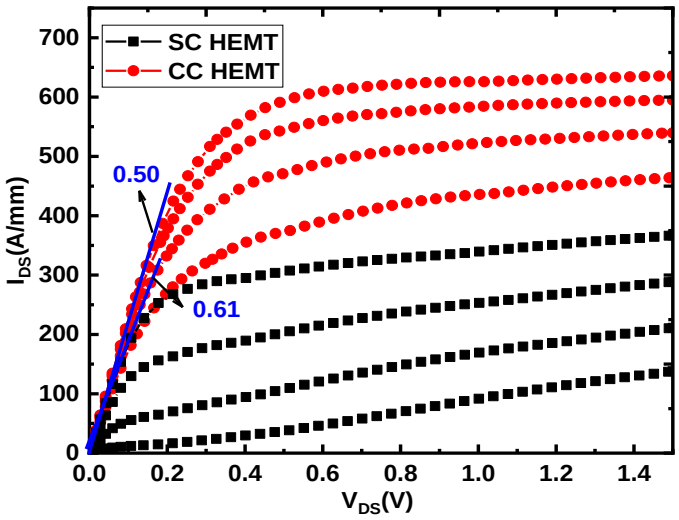

Fig. 5. The drain voltage-drain current curves at V_{GS} from 0 V to –0.4 V for the CC HEMT(black) and SC HEMT(red).

The transfer characteristics of SC HEMT and DC HEMT are shown in Fig. 6. It is obvious that the I_{DS} and transconductance of DC HEMT can be strengthened compared with that of SC HEMT. The structure with the double InGaAs/InAs channel shows the peak transconductance of 1019.7 mS/mm, which is 29.2% higher than that of SC HEMT. This means that the control of drain by the V_{GS} was improved for DC HEMT. The double InGaAs/InAs channel could be effectively confine the electron in the main channel, which led to the increase of peak transconductance. In addition, the threshold voltages are -0.8 V and -0.52 V for the DC HEMT and SC HEMT, respectively, which moved negatively. The threshold voltage moved negatively for DC HEMT, due to the double quantum well at InGaAs/InAs channel and the slightly higher electron concentration.

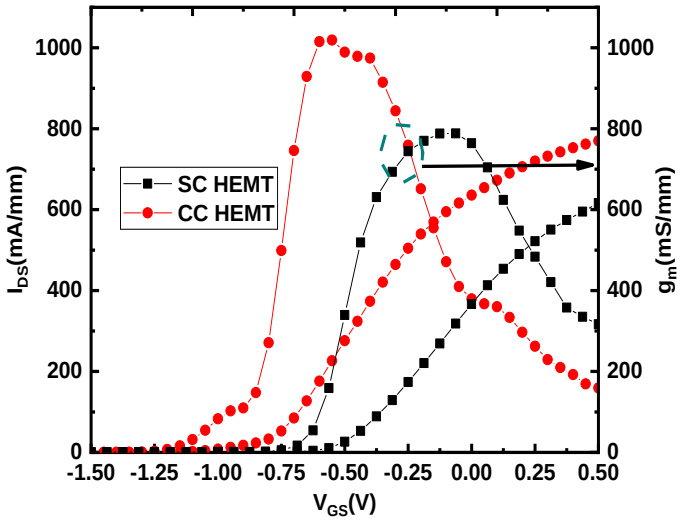

Fig. 6. The transfer characteristics at V_{DS}=1.5 V for the CC HEMT(black) and SC HEMT(red).

The subthreshold characteristics for the SC HEMT and CC HEMT were shown in Fig. 7. It can be seen that the subthreshold slope (SS) was 166.7 mV/decade for the SC HEMT, which was higher as compared to 103.5 mV/decade found in DC HEMT. For drain-induced-barrier-lowering (DIBL), the DIBL of SC HEMT and DC HEMT were 137.9 mV/V and 107.9 mV/V, respectively. Therefore, DC HEMT achieved much lower value of SS and DIBL, which showed that a more favorable electrostatic gate control was obtained by double InGaAs/InAs channel.

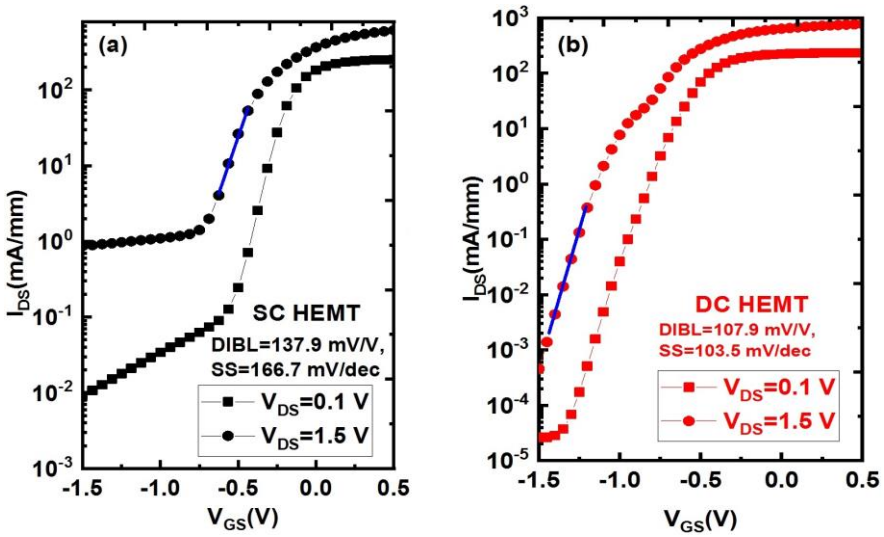

Fig. 7. Subthreshold characteristics of the SC HEMT and DC HEMT.

For the high frequency devices, f_T and f_{max} are the most important parameters. f_T determines the switching speed of the digital circuit and f_{max} affects the device power gain of the analog circuit. The variation of f_T and f_{max} with the change of V_{GS} for different channel structures

were discussed by the small-signal AC simulation, as shown in Fig. 8. It can be seen that the f_T and f_{max} were improved by the double InGaAs/InAs channel. The peak value of f_T and f_{max} for the CC HEMT are 392.6 GHz and 758.7 GHz, while the peak value of f_T and f_{max} for the SC HEMT are 262.6 GHz and 553.0 GHz. Compared with the SC HEMT, the peak value of f_T and f_{max} were increased by 49.6% and 37.2% for CCHEMT. This is mainly due to the fact that the gm of CC HEMT is higher than taht of the SC HEMT.

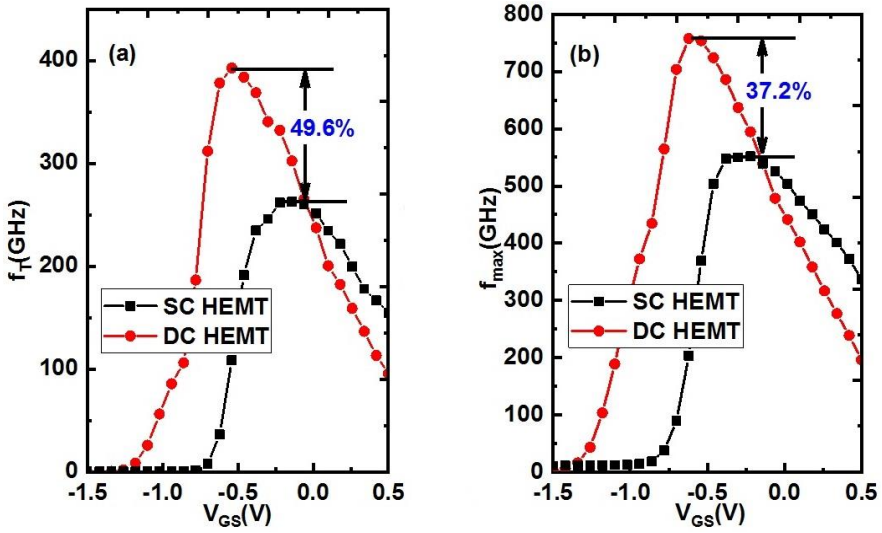

Fig. 8. Variation of (a) f_T and (b) f_{max} with respect to V_{GS} for a CC HEMT and SC HEMT.

4. Conclusions

In summary, the effect of double InGaAs/InAs channel structure on the DC and RF characteristics of InP-based HEMT is analysed by the numerical simulation. The better performance of DC HEMT was achieved due to better confinement of electron in the channel through the increase of conduction band offset. Compared with the SC HEMT, the saturated channel current and the peak value of transconductance were 73.4% and 29.2% higher than those of SC HEMT, respectively. The lower value of SS and DIBL for DC HEMT were obtained and showed a favorable electrostatic gate control characteristic. In addition, the superduper frequency characteristics were also obtained. The peak value of f_T and f_{max} increased by 49.6% and 37.2% for DC HEMT. The results demonstrated that the DC HEMT showed the attractive aspects for future analog and high-frequency RF applications.

Acknowledgements

This research was funded by the Project funded by China Postdoctoral Science Foundation (No.2021M700685), Key Scientific Research Projects of Colleges and Universities in Henan Province (No.21B140006, 22A510016), National Scientific Research Project Cultivation Fund of

Huanghuai University (No. XKPY-202103, XKPY-202106, XKPY-202006), Henan Provincial Science and Technology Research Project (222102310286).

References

[1] J. Ajayan, D. Nirmal, R. Mathew, D. Kurian, P. Mohankumar, L. Arivazhagan, D. Ajitha, Materials Science in Semiconductor Processing, 128, 105753(2021); https://doi.org/10.1016/j.mssp.2021.105753

[2] Y. Chen, L. A. Yang, Z. Jin, Y. B. Su, Y. Hao, IEEE Transactions on Elecron Devices, 68(5), 2226(2021); https://doi.org/10.1109/TED.2021.3066139

[3] S. X. Sun, Y. H. Zhong, H. Y. Mei, R. X. Yao, F. J. Chen, Y. X. Li, Y. F. Hu, Journal of Ovonic Research, 17(2), 137(2021).

[4] L. J. He, B. Y. Zhao, C. Y. He, Z. Y. Xie, J. S. Zhang, W. Z. Chen, Microelectronics Journal, 118, 105261(2021); https://doi.org/10.1016/j.mejo.2021.105261

[5] D. C.o Ruiz, D. Han, G. Bonomo, T. Saranovac, O. Ostinelli, C. R. Bolognesi, Physica Status Solidi A, 218(3), 2000191(2020); https://doi.org/10.1002/pssa.202000191

[6] J. N. Deng, J. H. Shao, J. Wan, B. R. Lu, Y. F. Chen, Microelectronic Engineering, 208, 54(2019); https://doi.org/10.1016/j.mee.2019.02.004

[7] S. X. Sun, X. L. Fu, L. Wang, M. E, J. J. Yi, R. X. Yao, X. Y. Zheng, H. T. Wu, F Liu, Y. H. Zhong, Y. X. Li, P. Ding, Z. Jin, Journal of Ovonic Research, 17(5), 411(2021)

[8] H. B. Jo, D. Y. Yun, J. M. Baek, J. H. Lee, T. W. Kim, D. H. Kim, T. Tsutsumi, H. Sugiyama, H. Matsuzaki, Applied Physics Express, 12(5), 054006(2019); https://doi.org/10.7567/1882-0786/ab1943

[9] H. B. Jo, J. M. Baek, D. Y. Yun, S. W. Son, J. H. Lee, T. W. Kim, D. H. Kim, T. Tsutsumi, H. Sugiyama, H. Matsuzaki, IEEE Electron Device Letters, 39(11), 1640(2018).

[10] J. Ajayan, D. Nirmal, P. Mohankumar, L. Arivazhagan, Silicon, 12, 1225(2020); https://doi.org/10.1007/s12633-019-00226-1

[11] J. N. Yao, Y. C. Lin, M. S. Lin, T. J. Huang, H. T. Hsu, S. M. Sze, E. Y. Chang, Solid State Electronics, 157, 55(2019); https://doi.org/10.1016/j.sse.2019.03.060

[12] P. Ding, C. Chen, Muhammad Asif, X. Wang, J. B. Niu, F. Yang, W. C. Ding, Y. B. SU, D. H. Wang, Z. Jin, IEEE Journal of the Electron Devices Society, 6, 49(2018); https://doi.org/10.1109/JEDS.2017.2765349

[13] J. Ajayan, T. Ravichandran, P. Prajoon, J. Charles Pravin, D. Nirmal, Journal of Computational Electronics, 17, 265(2018); https://doi.org/10.1007/s10825-017-1086-4

[14] J. Ajayan, T. Ravichandran, P. Mohankumar, P. Prajoon, J. Charles Pravin, D. Nirma, IETE Journal of ResearchVolume, 67(3), 366(2021).

[15] S. X. Sun, L. H. Ma, C. Cheng, C. Zhang, Y. H. Zhong, Y. X. Li, P. Ding, Z. Jin, Physica Status Solidi A, 214(10), 1700322(2017); https://doi.org/10.1002/pssa.201700322

[16] S. X. Sun, H. F. Ji, H. J. Yao, S. Li, Z. Jin, P. Ding, Y. H. Zhong, Chinese Physics B, 25(10), 108501(2016); https://doi.org/10.1088/1674-1056/25/10/108501

[17] S. Tewari, A. Biswas, A. Mallik, IEEE Transactions on Elecron Devices, 63(6), 2313(2016);

https://doi.org/10.1109/TED.2016.2548518

[18] J. Ajayan and D. Nirma, Journal of Semiconductors, 38(4), 044001(2017); https://doi.org/10.1088/1674-4926/38/4/044001

[19] J. Ajayan, T. D. Subash, D. Kurian, Superlattices and Microstructures, 109, 183(2017); https://doi.org/10.1016/j.spmi.2017.05.015